Aeroservoelastic Tailoring for Lateral Control Enhancement

Terrence A. Weisshaar* and Changho Nam†
Purdue University, West Lafayette, Indiana 47907

The purpose of this paper is to illustrate the application of an automated optimization approach to the integrated structural and control design of an aircraft wing and its control surface. The performance index or cost function for optimization is the aileron hinge moment required to sustain a specified terminal roll rate at a chosen design speed at which aeroelastic effects are significant. The design variables used for aileron hinge-moment minimization are the aileron flap-to-chord ratio; the location of the aileron with respect to the roll axis; and the orientations of three advanced composite plies comprising 60% of the wing structure. In addition to presenting the results of the optimization process itself, the study examines the effects of aileron location and advanced composite ply orientation on the terminal roll rate and aileron hinge moment. Optimization is seen to involve a compromise between a laminated structure/aileron combination that is effective in creating large rolling moments and one that minimizes the damping-in-roll. These two requirements are in conflict; the optimization driver must locate a compromise design point by moving the control surface and changing its size while also creating a suitable structural design.

Introduction

THE need for effective aircraft lateral control for rolling and turning is as old as powered flight itself. The effectiveness of the aerodynamic surface used for this control depends on a long list of parameters, including the following: Mach number, control-surface shape, size, and location on the wing, and the aeroelastic characteristics of the aircraft at a particular flight condition.

The purpose of this paper is to examine a procedure for integrated optimal structural design and control surface design. The use of the term "optimal" implies a measure of goodness that is commonly referred to as the performance index. This performance index will be a measure of the aileron hinge moment required to achieve a specified terminal roll rate at a certain airspeed, called the design airspeed.

Three structural design freedoms available for optimization are the orientations of advanced composite laminate plies that comprise 60% of a 10-layer platelike structure of a 30 deg sweptback wing. The control design parameters are the aileron flap-to-chord ratio and the spanwise location of the aileron on the wing. The total spanwise length of the aileron is fixed to be 30% of the wing semispan. Since this is a multidisciplinary optimization study, several facets of aileron roll effectiveness will be reviewed before the discussion of the analysis/optimization procedure.

Background

Among the problems solved by the Wright Brothers before their first flight were provisions for three-axis control of the aircraft; the fact that the Wright Flyer was statically unstable in pitch and roll created a challenging situation.[1] To create the necessary rolling moment for active roll stabilization, and to bank the aircraft, they used wing torsional flexibility to distort the wing; this distortion is referred to as "wing warping."

Although the Wright Flyer biplane structure was relatively stiff in bending, intentional torsional flexibility tailored into the wing allowed the prone pilot to use hip movement to move a control cradle, connected to a wire apparatus, to create differential wing twist to warp the wings. The increased lift on one side and reduced lift on the other created the required roll moment. Excessive torsional flexibility would be desirable from the point of view of the powered actuator (Wilbur or Orville), but undesirable from a structural and aeroelastic point of view. However, the proper integration of structural stiffness into the Wright Flyer control design led to its success.

Ailerons quickly replaced wing warping as roll control devices. The amount of aerodynamic rolling moment generated by a unit differential deflection of a control surface is proportional to dynamic pressure as long as the wing does not deform. This roll moment causes the roll rate, denoted by p, to build rapidly. Damping-in-roll, created by wing rolling motion, opposes unchecked rolling motion. As a result, roll velocity will reach a steady-state or terminal roll rate when the damping-in-roll moment equals the roll moment created by the ailerons. The damping-in-roll moment that opposes rolling motion is proportional to roll rate p and airspeed V. Without wing distortion, the terminal roll rate per unit δ_0 is proportional to the airspeed, as indicated on the left side of Fig. 1.

The same aileron deflection that provides an increase in lift on the wing section also produces a nose-down twisting mo-

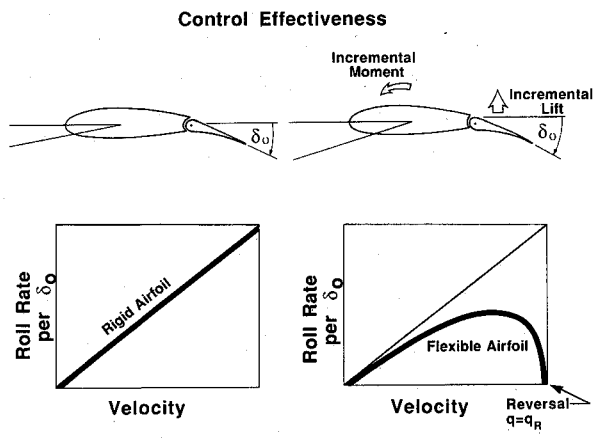

Fig. 1 Control effectiveness as a function of airspeed for a rigid and a flexible airfoil. Effectiveness is the ability of an aileron to generate a terminal roll rate p for a unit aileron displacement δ_0.

Received March 5, 1988; revision received Oct. 24, 1988. Copyright © 1989 by T. A. Weisshaar and C. Nam. Published by the American Institute of Aeronautics and Astronautics, Inc., with permission.

*Professor, School of Aeronautics and Astronautics. Associate Fellow AIAA.

†Graduate Research Assistant. Student Member AIAA.

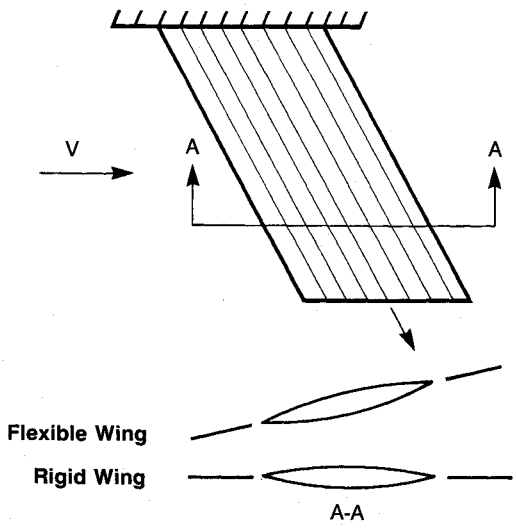

Fig. 2 Aeroelastic wash-out of a flexible swept wing caused by upward bending under the load due to an aileron.

ment that is proportional to dynamic pressure. A combination of twisting flexibility and high dynamic pressure can produce a substantial nose-down aeroelastic twist that reduces both the airfoil angle of attack and the net lift generated by the aileron. As a result, the flexible airfoil produces a smaller rolling moment, as is indicated qualitatively on the right side of Fig. 1.

At the reversal dynamic pressure q_R, the lift generated by the aileron deflection is exactly counterbalanced by that produced by the aileron-induced twist so that a force couple, but no net lift, results. At dynamic pressures larger than the reversal dynamic pressure, a pilot stick input that would normally produce a rolling response to the left produces roll to the right; above this dynamic pressure, the controls are said to be "reversed."

Aileron reversal occurred on a number of early unswept monoplanes with low torsional stiffness. These difficulties spawned a number of significant qualitative and quantitative studies of aileron effectiveness beginning after World War I and continuing up to the present time. Cox and Pugsley[2] were among the early researchers who studied the aeroelastic behavior of unswept, cantilever monoplane wings with ailerons of different sizes. As a result of their research, they suggested the terminal roll rate per unit aileron deflection (p/δ_0) as a good measure of the lateral maneuverability of a flexible airplane because the time required to achieve a specified roll rate decreases as p/δ_0 increases. However, Cox and Pugsley also suggested the ratio p/V as an even better measure of aileron performance when the objective is to achieve a certain roll rate in a minimum flight distance, since a large value of p/V is associated with a shorter elapsed distance. Their recommendations were in contrast to an earlier study by Ogawa[3] who used maximum angular acceleration as a measure of roll effectiveness for a rigid aircraft.

Cox and Pugsley also examined the interaction between control-system geometry (in their case aileron surface area and aileron length) and roll effectiveness. They found that, for their configuration, an aileron that begins at the wing/fuselage junction and extends outward 70% of the wing semispan is best. Earlier work by Irving et al.[4] had examined different aileron planform proportions and measured aileron efficiency by computing the ratio of aileron rolling moment-to-aileron hinge moment required to achieve a prescribed roll moment. Along the same lines, Glauert[5] measured aileron performance by defining it as rolling moment squared, divided by aileron hinge moment. He concluded that the best aileron span on an unswept wing is two-thirds of the total semispan. In his study, aileron chord did not have much influence on this "performance index" when aileron chords of only 20 to 30% of the planform chord were considered. Glauert also suggested that the ratio of p^2-to-hinge moment be used as a criteria if large values of p are the objective of the aileron design.

During World War II, Harmon[6] updated the studies of Cox and Pugsley and included flight test data for a P-47C fighter aircraft. He also examined the role of sideslip of the aircraft in reducing roll effectiveness of the ailerons.

These early studies did not address swept-wing aircraft roll effectiveness. After World War II, the development of high-speed, swept-wing aircraft added a new dimension to control effectiveness. Sweptback wing bending, combined with the nose-down twisting effect shown in Fig. 1, further aggravates reversal. As illustrated in Fig. 2, upward bending along a sweptback spanwise axis produces a streamwise geometrical effect identical to a nose-down torsional rotation. As a result, a downward aileron displacement to increase lift on a swept wing accentuates adverse twisting distortion. Post-World War II aircraft with high aspect ratio swept wings encountered roll effectiveness difficulties sufficient to lead to the adoption of alternative surfaces to replace ailerons as lateral control surfaces.[7]

Despite the mutual interaction between the control-surface deflection and swept-wing flexibility, control ineffectiveness is still perceived to be a structural problem. Until the early 1970s, the only engineering measures available to counter control ineffectiveness were reduced airspeed, limited maneuverability, or increased structural stiffness. This is no longer true.

The late 1960s and 1970s witnessed the development of reliable advanced composite materials. In addition to extreme strength and stiffness, these laminated materials allow the designer the freedom to tailor the laminate-ply orientation to develop optimal stress paths within the material. They also allow the coupling together of deformation modes, such as spanwise bending and twist, without adversely affecting strength. The result is an adaptable or "user friendly" structure that naturally redistributes aerodynamic loads, depending on the laminate geometry and the flight speed. This design process is referred to as aeroelastic tailoring.

References 8 and 9 provide an extensive background and history of aeroelastic tailoring, including roll effectiveness studies. Reference 10 provides an example of a state-of-the-art look at aeroelastic tailoring efforts in an industrial setting. Because of the range of laminate design possibilities provided by a multitude of laminate orientations and stacking sequences, there exists the potential, and perhaps the necessity, for formal optimization procedures for laminate design.

The design of an efficient structural arrangement to enhance control in an aeroelastic environment recognizes the strong coupling between aeroelasticity and control devices. This interaction is referred to as aeroservoelasticity, of which aileron effectiveness is a subset. As a result of these interactions, an integrated design approach is advisable, if not required.

The term "integrated" implies a cooperative effort with a common goal. The definition of a common goal is not always easy when diverse disciplines are to be integrated. Fortunately, in this case, given the historical definitions of aileron efficiency, it is relatively easy to define a measure of efficiency that will satisfy both the structures and control design participants. As discussed previously, hinge moment is a measure of aileron efficiency at a given terminal roll rate. In addition, as suggested by Sensburg and Schmidinger,[11] the hinge-moment requirement determines the actuator weight. Weight reduction is of great importance in aircraft design so, as a result, hinge-moment minimization was chosen as the performance index.

In the next section, an aeroservoelastic design problem is defined with a measure of aileron hinge moment as the performance index and with a set of interdisciplinary design variables. We will then solve this problem and examine and interpret the results.

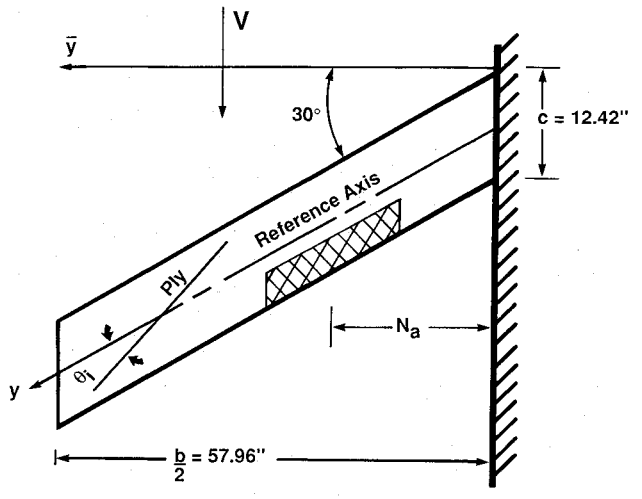

Fig. 3 Planform for aeroservoelastic optimization study showing geometry, reference axis, and laminate orientation θ_i.

Optimization-Performance Index and Design Variables

Shown in Fig. 3 is the wing planform used for this study. An aileron with a length equal to 30% of the wing semispan is attached. Its spanwise location N_a and the aileron flap-to-chord dimension are control design variables. A high-aspect-ratio laminated plate with 10 plies of constant-thickness graphite/epoxy material provides wing stiffness. The angular orientations θ_i of three upper (and lower) plies of this symmetrically laminated plate complete the list of design variables. Because the plate is symmetrical through the thickness, 60% of the plate structure is tailorable or subject to design modification. This wing is required to develop a terminal roll rate of 1.5 rad/s at an airspeed of 152 mph at sea level. Because of aeroelastic interaction, the aileron deflection angle required to achieve this roll rate will change markedly with laminate orientation.

The wing structure is characterized as a one-dimensional beam with spanwise bending stiffness EI, torsional stiffness GJ, and a bend/twist stiffness cross-coupling parameter K. These three stiffness parameters are measured along the spanwise swept reference axis in Fig. 3 and are functions of the laminate geometry and material characteristics. The parameter K determines the twist rate produced by a spanwise bending moment or, alternatively, the bending curvature caused by a spanwise twisting moment.[9] An orthotropic laminate design laid up along the y axis in Fig. 3 will produce a value of $K = 0$. An important effect of stiffness cross-coupling is that it can significantly change the position of the streamwise locus of centers of twist (the flexural axis) for the beam. Airloads applied downstream of the flexural axis will rotate the wing nose down.[9]

An accurate description of the spanwise lift distribution caused by aileron deflection, rolling motion, and structural deformation is required. The computational method chosen for this study is based on that outlined by Gray and Shenck.[12] Reference 12 presents not only an aerodynamic model, but also develops a flexibility matrix for a structural stiffness model. Modifications to that structural model to account for laminated beam bend-twist deformation cross-coupling are developed in Ref. 13. This procedure was programmed into a computer code, CWINGSM, and used for this study.

A set of simultaneous linear algebraic equations describes the aeroelastic response of the wing to steady-state aileron input. This is a result of discretizing the planform into a set of spanwise segments. Horseshoe vortices are attached at the quarter-chord-line of each of these panels. The accuracy of this discrete representation depends partially on the number of panels used. For the present study, 20, equal-width, spanwise panels were used to represent the wing semispan in Fig. 3. In addition, the spanwise airload distribution was restricted to antisymmetrical rolling motion about the longitudinal centerline.

The lift intensity p_i (note that with the subscripting, p_i is lift per unit length, not roll rate) acting on each panel is related to the angles of attack along the wing. A relationship between the vector of panel lift intensities $\{p_i\}$ and the local panel angle of attack α_i is written as follows:

$$1/q[A_{ij}]\{p_j\} = \{\alpha_i\} \tag{1}$$

The matrix $[A_{ij}]$ is a square matrix (of order $n \times n$ where n is the number of panels) of aerodynamic influence coefficients, whereas q represents the flight dynamic pressure.

The elements A_{ij} are functions of planform geometry and "known" values of each panel's two-dimensional lift-curve slope. If the vector of local angles of attack α_i is specified, then the lift distribution may be found simply by premultiplying Eq. (1) by $q[A_{ij}]^{-1}$. If aeroelastic interaction is included, then the vector $\{\alpha_i\}$ is unknown, since the loads p_i will cause surface distortion that will change α_i.

For a roll maneuver, the vector of panel angles of attack is a linear combination of three characteristic types of angles of attack, each associated with a specific part of the maneuver. This vector is expressed as

$$\{\alpha_i\} = \{\alpha_s\} + pb/2V\{\bar{y}_i\} + \{\alpha_c\} \tag{2}$$

where $\bar{y}_i$ is the nondimensional distance from the roll axis to the panel midspan, defined as $\bar{y} = 2\bar{y}/b$. The elements of Eq. (2) are $\{\alpha_s\}$, the streamwise angles of attack due to structural bend/twist deformation; $pb/2V\{\bar{y}_i\}$, the spanwise angles of attack due to rolling motion p at airspeed V; and $\{\alpha_c\}$, the apparent aerodynamic twists due to control deflection.

The streamwise angles of attack $\{\alpha_s\}$ caused by the bending and twisting of the planform are related to the lift intensity distribution vector through a flexibility matrix $[C_{ij}]$, developed in Ref. 13, as follows:

$$\{\alpha_s\} = [C_{ij}]\{p_j\} \tag{3}$$

Upon substitution of Eq. (3) into Eq. (1), the following combination is created:

$$\left[1/q[A_{ij}] - [C_{ij}]\right] \triangleq [B_{ij}] \tag{4}$$

The matrix $[B_{ij}]$ is the aeroelastic flexibility matrix.

The solution for the airload distribution requires the inverse of $[B_{ij}]$; this matrix may be singular at certain critical values of q denoted as q_D. The lowest of these values corresponds to the clamped-wing divergence dynamic pressure.

The control-surface-induced spanwise angle-of-attack distribution $\{\alpha_c\}$ is due to two effects, one of which is purely geometrical, whereas the other depends on airfoil bend/twist flexibility. The deflection of a control surface located on any of the wing panels will cause a change in the apparent angle of attack of that panel by reorienting the zero lift line. This change is written as

$$\alpha_{c1} = \frac{\partial \alpha}{\partial \delta}\delta_0 \tag{5}$$

The derivative in Eq. (5) is written as

$$\frac{\partial \alpha}{\partial \delta} = \frac{\partial c_l}{\partial \delta}\left(\frac{\partial c_l}{\partial \alpha}\right)^{-1} = \frac{c_{l\delta}}{c_{l\alpha}} \tag{6}$$

The two-dimensional section derivative $c_{l\delta}$ is a function of a number of parameters, two of the most important being Mach number and the aileron flap-to-chord ratio.

Since control-surface deflection creates a twisting moment about the aerodynamic center at the quarter-chord of the panel, each control-surface panel is subjected to a twist per

unit length proportional to the product $qc_i^2 c_{m\delta}\delta_0$, where c_i is the panel chord. If the values of the two-dimensional, streamwise pitching-moment coefficient $c_{m\delta}$ are identical for each panel, then this component of the control-induced twist distribution may be written as

$$\{\alpha_{c2}\}' = q[E_{ij}]\{\gamma_i\}c_{m\delta}\delta_0 \tag{7}$$

The $[E_{ij}]$ matrix is a wing/aileron flexibility matrix that provides the streamwise wing twist distribution due to an initial streamwise pitching-moment distribution created by the ailerons along the wing span. Note that $[E_{ij}]$ determines the streamwise wing rotation due to a torque intensity distribution computed at the quarter-chord of each panel. The term $\{\gamma_i\}$ in Eq. (7) is a vector that controls and identifies which panels have aileron segments. If a panel (j) has no aileron, then γ_j is zero. If a panel has an aileron deflected down, then γ_i is equal to unity; an aileron deflected upward is identified by a negative unity value.

If we substitute Eqs. (5) and (7) into Eq. (1), the solution for $\{p_i\}$ is found to be

$$\{p_i\} = [B_{ij}]^{-1}\left\{\frac{pb}{2V}\{\bar{y}_i\} + q[E_{ij}]\{\gamma_i\}c_{m\delta}\delta_0 + \{\gamma_i\}\frac{\partial\alpha}{\partial\delta}\delta_0\right\} \tag{8}$$

The condition for steady-state roll moment equilibrium is found by summing panel roll moments over the entire span. With $\bar{y}_i$ as the distance from the roll axis to the center of a panel of width h_i, this condition is expressed as

$$\{\bar{y}_i\}^T\{p_i h_i\} = 0 \tag{9}$$

With Eq. (9) prescribing steady-state motion, $pb/2V$ and δ_0 are not independent. Placing Eq. (8) into Eq. (9) and solving for δ_0 give

$$\delta_0 = \frac{(-pb/2V)\{\bar{y}_i h_i\}^T[B_{ij}]^{-1}\{\bar{y}_i\}}{\{\bar{y}_i h_i\}^T[B_{ij}]^{-1}\left\{q[E_{ij}]\{\gamma_i\}c_{m\delta} + \{\gamma_i\}\frac{\partial\alpha}{\partial\delta}\right\}} \tag{10}$$

The numerator in Eq. (10) is the damping-in-roll moment generated by rolling motion. The term multiplying $pb/2V$ is referred to as C_{l_p} in aircraft stability and control literature.[14] The denominator is sometimes called the aileron rolling power (per unit aileron deflection). This term depends on wing stiffness as well as the aileron size and spanwise position, represented by $\{\gamma_i\}$. The matrix term $[B_{ij}]^{-1}$ appears in both the numerator and denominator of Eq. (10). In theory, the singularity that appears when $q = q_D$ will cancel out of Eq. (10) so that it cannot be relied on to detect wing aeroelastic divergence.

The first term in the denominator of Eq. (10) is the source of aileron reversal. Because of the camber changes associated with an aileron deflection, $c_{m\delta}$ will be negative and the first term in the denominator of Eq. (10) will become increasingly negative as q increases. As a result, the aileron rolling power will become zero at the reversal dynamic pressure. When this happens, δ_0, as given in Eq. (10), will tend to infinity.

If we define aileron effectiveness as $pb/2V/\delta_0$, then with $c_{m\delta}$ and $\partial\alpha/\partial\delta$ constant along the wing span, the expression for aileron effectiveness may be written as

$$\left.\frac{pb}{2V}\right|\delta_\alpha = \frac{\left(M_{m\alpha}\frac{\partial\alpha}{\partial\delta} + M_{m\delta}c_{m\delta}\right)}{(-D_R)} \tag{11}$$

The numerator in Eq. (11) is the aileron rolling power, whereas D_R is the damping in roll. Note that the term $(-D_R)$ is positive.

Turning to the hinge moment, we note that its use as a performance index has some potential drawbacks, since the hinge moment is a function of many diverse design parameters. Included among these parameters are aileron balance, trailing-edge shape, gap size, and geometry.[15] Etkin[14] notes that of all aerodynamic parameters required for a stability and control analysis, aileron hinge-moment coefficients are the most difficult to predict precisely. Reference 15 shows that hinge moments on trailing-edge controls may be nonlinear functions of angles of attack and flap deflection if the aileron rotation angle is too large.

These difficulties notwithstanding, a measure of hinge moment is proposed that, if not precisely equal to the hinge moment, still can be used to reflect the magnitude of the hinge moment. This measure is derived from the hinge moment predicted by two-dimensional aerodynamic theory for an airfoil with a trailing-edge control surface.[16] For the ith panel on the wing, the expression for the panel aerodynamic hinge moment is denoted as f_i and is given as

$$f_i = (\pi/4)\rho c_i^2\,(V/\pi)^2\,(T_5 - T_4 T_{10})h_i\beta_i \tag{12}$$

$$T_4 = -\cos^{-1}\epsilon + \epsilon\sqrt{1-\epsilon^2} \tag{13}$$

$$T_5 = -(1-\epsilon^2) - (\cos^{-1}\epsilon)^2 + 2\epsilon\sqrt{1-\epsilon^2}\cos^{-1}\epsilon \tag{14}$$

$$T_{10} = \sqrt{1-\epsilon^2} + \cos^{-1}\epsilon \tag{15}$$

In these latter equations, the symbol ϵ represents the distance, measured in wing semichords ($c_i/2$), between the aileron hinge line and the midchord of the airfoil.

In Eq. (12), the angle β_i represents the angle of incidence between the airstream and the aileron and is the sum of the aileron rotation δ_0; the panel structural twist; and the equivalent twist due to roll-induced velocity at that particular panel. If we know the total number and position of the spanwise segments to which ailerons are attached, the values of f_i for each panel may be computed and then added together to obtain the total hinge moment, denoted as H.

The optimization problem begins by defining the following constraint:

$$\frac{\left(M_{m\alpha}\frac{\partial\alpha}{\partial\delta} + M_{m\delta}c_{m\delta}\right)}{(-D_R)}\delta_0 - \left(\frac{pb}{2V}\right)_{\text{des}} = 0 \tag{16}$$

In Eq. (16) the term $(pb/2V)_{\text{des}}$ is a numerical value when p is 1.5 rad/s and the wing operates at the design velocity V. Equation (16) defines δ_0. The terms $\partial\alpha/\partial\delta$ and $c_{m\delta}$ are computed from relations consistent with those used to compute hinge moment; these are[16]:

$$\frac{\partial\alpha}{\partial\delta} = \frac{1}{\pi}T_{10} \tag{17}$$

$$c_{m\delta} = -\left(\frac{1+\epsilon}{2}\right)\sqrt{1-\epsilon^2} \tag{18}$$

During the search for the minimum hinge moment, the flap-to-chord ratio, given as $\bar{c} = \frac{1}{2}(1-\epsilon)$, is required to lie between specified limits. Because of geometric constraints, the aileron midspan position cannot be less than 15% of the span, nor greater than 85% of the span since the aileron span is itself 30% of the wing span.

The optimization problem reads as follows:

Minimize

$$H(x_j) = \sum_{n=1}^{6} f_n \qquad (j = 1, 5) \tag{19}$$

subject to

$$g_i(x_j) \le 0 \qquad (i = 1, 2, 3, 4) \tag{20}$$

The symbol x_j represents the five design variables (three laminate orientation angles θ_i, aileron spanwise position N_a, and flap-to-chord ratio $\bar{c}$), whereas g_i represents the four inequality constraints on aileron spanwise location and chordwise geometry. Six of 20 wing panels contain aileron segments.

Two different optimization approaches were used for this problem. One approach views the constrained optimization problem as a sequence of unconstrained minimization problems by using an interior penalty function method.[17] This procedure defines a pseudoperformance index Φ as the sum of the hinge moment H and a weighted sum of penalty functions that incorporate constraints. This objective function is

$$\Phi(x_i, r_p) = H(x_i) + r_p s(x_i) \tag{21}$$

where

$$s(x_i) = -\sum_{j=1}^{4} \frac{1}{g_j(x_i)} \tag{22}$$

The choice of a value for the multiplicative constant r_p is left to the analyst.

In theory, the function $\Phi(x_i)$ converges to the optimal design from design points within the feasible design region. The design itself can approach the constraints, but violations are never allowed because Eq. (22) imposes heavy penalties near constraint boundaries where g_i is zero. During successive design cycles, as design progresses, the constant r_p is redefined to be smaller and smaller. Note that $\Phi(x_i, r_p)$ is discontinuous at the constraint boundaries. The Davidon-Fletcher-Powell method, in conjunction with a cubic interpolation method, was chosen to implement this design optimization approach.[17]

A second, more restrictive optimization approach proved valuable during the initial stages of this study. For this portion of the study, the spanwise position of the aileron was treated as a design parameter, together with flap-to-chord ratio. As a result, the inequality constraints could be discussed so that only the orientations of the structural plies remained. The Fletcher-Reeves method was used in conjunction with a cubic interpolation method to select a one-dimensional step size.[17] The problem consisted of a series of unconstrained searches, each with different aileron spanwise positions.

Both optimization procedures require sensitivity derivatives, in particular, derivatives of hinge moment with respect to the laminate design variables θ_i, aileron midspan position N_a, and the flap-to-chord ratio. Expressions for these derivatives were derived analytically by differentiation of the matrix equations discussed previously. This approach permits the development of derivatives that provide the change in hinge moment due to a change in aileron position (a spacial derivative) and the change in hinge moment caused by a change in laminate orientation (a structural derivative). The expressions for sensitivity derivatives were then programmed and attached as subroutines to the existing analysis code, CWINGSM, to accomplish the optimization.

Study Results

To begin the study, we choose the approach in which the spanwise aileron position and its flap-to-chord ratio are fixed design parameters so that the structural optimization process may be isolated and examined. Two sets of initial design conditions involving the values of the three ply angles were considered. In the first case, all three plies were oriented initially at angles 20 deg forward of the reference axis ($\theta_1 = \theta_2 = \theta_3 = -20$ deg) to provide a wash-out (bend-up/twist-down) initial design point. In the second case, all three ply orientations were initialized at angles 80 deg aft of the reference axis ($\theta_1 = \theta_2 = \theta_3 = 80$ deg) to provide a strong initial wash-in (bend-up/twist-up) design. In each case, a different optimum laminate design was located by the unconstrained optimization procedure.

First of all, consider Fig. 4, which shows the minimum hinge moment obtained after structural optimization plotted against aileron spanwise position when the flap-to-chord ratio is 10%. The curve labeled "wash-out laminate" is that obtained when $\theta_i = -20$ deg is chosen as an initial starting point. For reference, the hinge moment associated with the nonoptimal orthotropic structure ($\theta_1 = \theta_2 = \theta_3 = 0$ deg) is also plotted in Fig. 4. For the initial points chosen, the optimization driver, after only two or three cycles, will locate a minimum hinge moment whose final laminate orientations θ_1, θ_2, and θ_3 are nearly equal. This design cycle history for a typical cycle is shown in the insert to Fig. 4. The values of θ_i associated with the minimum hinge moments in Fig. 4 are plotted in Fig. 5. Although these three angles begin as equal angles and end as equal angles, they were observed to be different during the design "process."

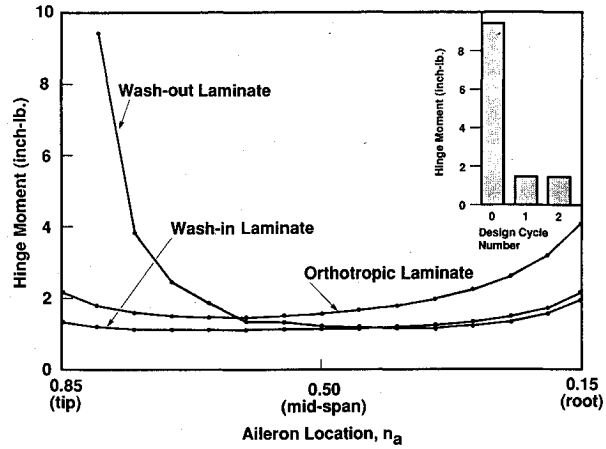

Fig. 4 Minimum hinge moment H vs aileron nondimensional spanwise locations $n_a = 2N_a/b$ resulting from structural design optimization. Flap-to-chord ratio c is fixed at 0.10.

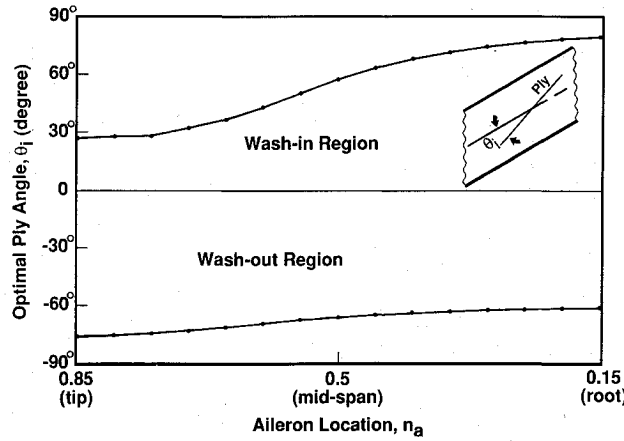

Fig. 5 Laminate orientations θ_1, θ_2, θ_3 associated with locally minimum hinge moment H plotted in Fig. 4. Flap-to-chord ratio $\bar{c}$ is 0.10.

A different minimum hinge moment result is found when $\theta_i = 80$ deg is used to create a wash-in starting point. The final optimum values of θ_i are also nearly equal and are shown plotted against aileron position in the wash-in region of Fig. 5.

Figure 4 seems to indicate that, when restricted to a certain flap-to-chord ratio and aileron position, the optimization driver, if presented with an initial wash-in design, usually will choose a wash-in design to create a minimum hinge moment. Similarly, an initial wash-out starting point yields minimum hinge-moment design with structural wash-out characteristics. Since the global minimum is the lower of the two curves in Fig. 4, when the aileron is located outboard, a structural design that emphasizes wash-in will produce the lowest actuator hinge moment. Structural wash-in creates a favorable aeroelastic coupling situation in which upward-bending deflection is accompanied by nose-up twist. This increases the aerodynamic effectiveness of the surface and seems to indicate that

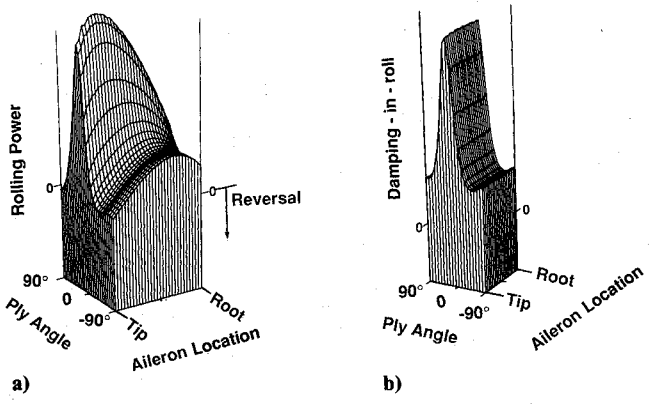

Fig. 6 a) Aileron rolling power vs common ply orientation θ_i and aileron nondimensional spanwise location $n_a = 2N_a/b$. Flap-to-chord ratio is 0.10. b) Damping-in-roll vs θ_i and n_a.

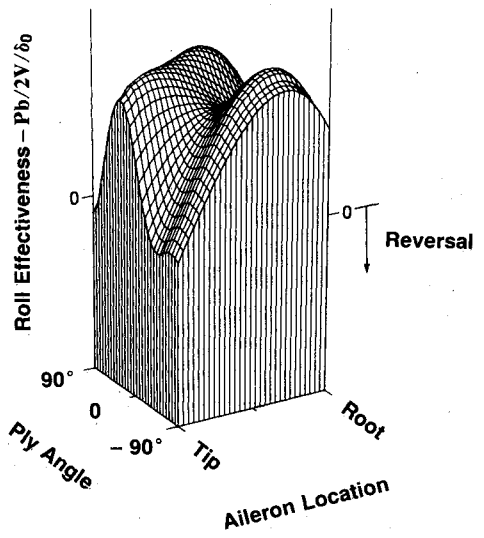

Fig. 7 Aileron effectiveness $pb/2V/\delta_0$ vs common ply orientation θ_i and aileron nondimensional spanwise position $n_a = 2N_a/b$. Flap-to-chord ratio is 0.10.

favorable bending of the wing due to aileron-induced lift is of more importance than adverse twisting caused by the aileron. In effect, the flexible 30-deg swept wing behaves, aeroelastically, more like a wing with a smaller sweep angle.

When the aileron is located outboard, the optimization procedure with the wash-out design starting point yields a design with a hinge moment that, while locally minimal, is still quite large. However, when the aileron is located at the midspan position, the optimal wash-in and wash-out designs, although structurally quite different, lead to nearly (or, in one case, exactly) the same hinge moment. When the aileron is placed further inboard, the wash-out design produces an optimum hinge moment that is slightly better than its wash-in counterpart.

To investigate the reasons for these results, the optimization driver was "disconnected" and parameter variations examined. For this special investigation, all three plies were restricted to have the same orientation and the aileron flap-to-chord ratio was fixed, as before, to be 10%. Figure 6 shows carpet plots of a) the aileron rolling power and b) damping in roll, plotted against laminate-ply angle and aileron spanwise position. Note that for plotting convenience, the negative value of D_R is plotted. Although D_R is not a function of aileron position, it is presented as such to create a common format in Fig. 6.

Figure 6a indicates that maximum aileron rolling power is obtained when the aileron is placed in an outboard position and the ply orientation is in the wash-in region, (0 deg < θ < 90 deg), near $\theta = 20$ deg. However, this type of laminate also creates the maximum (negative) damping in roll. This near coincidence of maxima occurs because the same aeroelastic effects that increase the aileron rolling power also increase the effectiveness of the lifting surface to generate damping in roll. Figure 6 indicates that a design compromise is necessary. Such behavior had been observed previously in a study by Niblett.[18]

Figure 7 shows the result when the quantities in Fig. 6 are combined to create a plot of aileron effectiveness [Eq. (11)]. Local maxima are seen to occur when the aileron midspan position is located about one-quarter of the span outboard of the wing root. The local maxima in the wash-in and wash-out regions are defined more clearly from a contour plot of aileron effectiveness shown in Fig. 8.

Figure 8 shows that maximum roll rate can be achieved with either a wash-in or a wash-out laminate. This figure indicates that a broad plateau exists in the wash-in region and that reversal (the dashed lines) occurs when the aileron is near the tips of the wash-out laminate. Figure 9 shows a contour plot of the hinge moment required to achieve a terminal roll rate of 1.5 rad/s at the design airspeed, plotted against laminate-ply orientation θ_i and nondimensionalized aileron spanwise position n_a. A local minima is located near (but, not at) the point where a local maximum aileron effectiveness occurs. The sec-

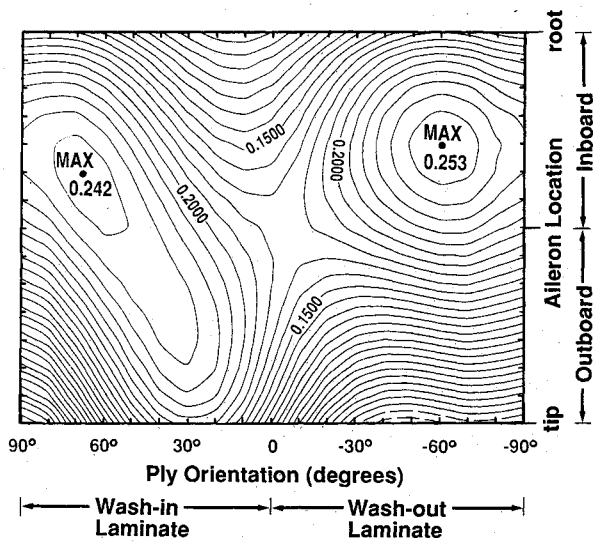

Fig. 8 Contour plot of aileron effectiveness $pb/2V/\delta_0$ vs common ply orientation θ_i and aileron location $n_a = 2N_a/b$.

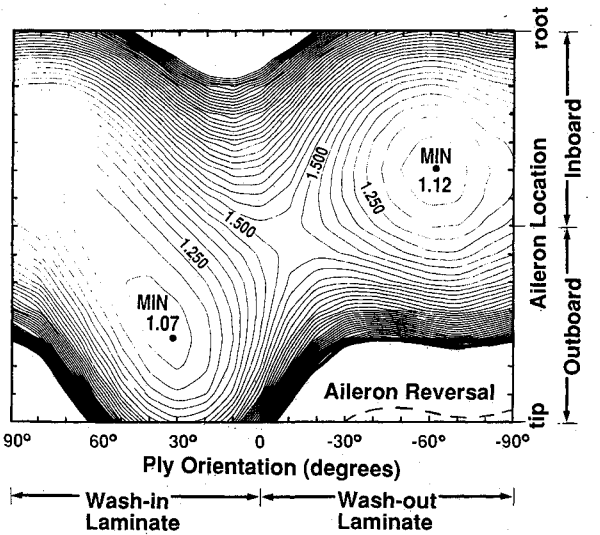

Fig. 9 Contour plot of hinge moment H vs aileron spanwise location $n_a = 2N_a/b$ and common ply orientation θ_i.

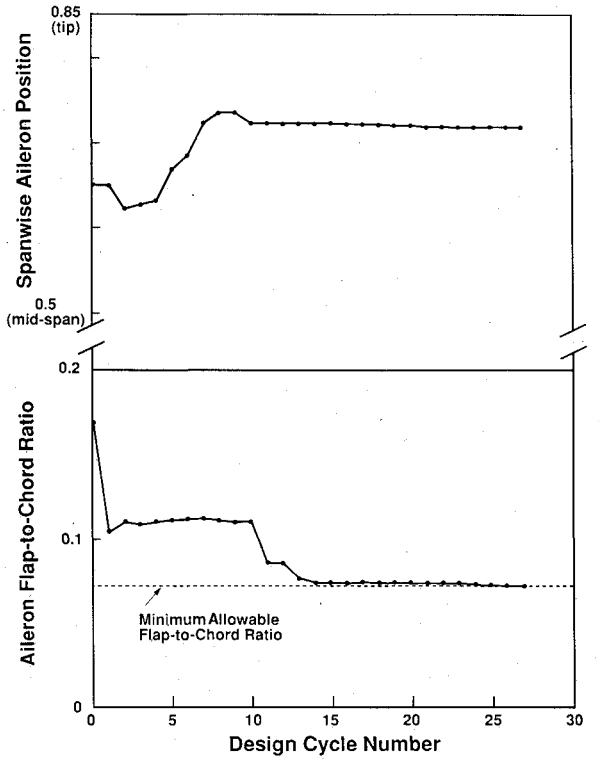

Fig. 10 Flap-to-chord ratio and aileron location vs design cycle, using the full set of design variables for the optimization problem.

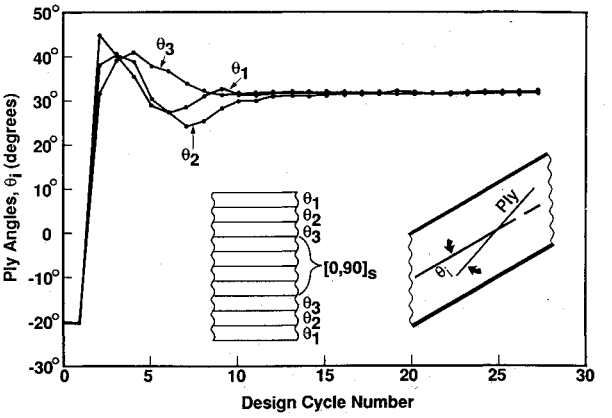

Fig. 11 Ply orientations θ_i vs design cycle during structure/control optimization.

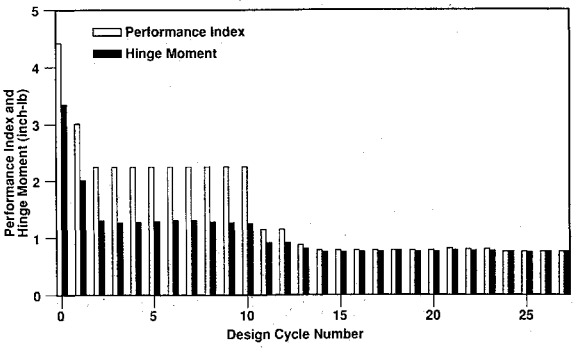

Fig. 12 Performance index Φ and hinge moment H plotted against design cycle when the five design variables are used in an integrated optimization procedure.

ond local (and global) minimum hinge moment is located some distance away from the location associated with the local maximum aileron effectiveness in the wash-in region, but still on the plateau observed in Fig. 8. The closely spaced contours associated with the outboard aileron region reveal an extremely large gradient of hinge moments consistent with the approach of aileron reversal. The aileron reversal point (where hinge moments are "infinite") is indicated by a dashed line in the lower right corner of Fig. 9.

These results indicate that a harmonious combination of structural stiffness and control surface size and location is likely to encounter the need for compromise between the ability to create a rolling moment (aileron rolling power) and the ability to provide low damping-in-roll. The first objective requires swept-wing lift effectiveness, whereas the second requires lift ineffectiveness. The additional requirement that the surface distortion and aileron rotation do not create excessive moments on the aileron actuator will further modify the outcome.

When all design variables are included in the optimization problem, the functional Φ defined in Eq. (21) is minimized. Figure 10 shows the values of the flap-to-chord ratio and aileron location as hinge-moment minimization progresses. From an initial value of about 17%, the flap-to-chord ratio declines until it reaches the minimum constraint boundary of 7.5%. The aileron spanwise location converges quite rapidly to its final position with the aileron midspan located about 70% outboard of the wing root. Note that the position labeled (tip) in Fig. 10 corresponds to $n_a = 0.85$.

Figure 11 tracks the orientations of the laminate-ply angles θ_1, θ_2, and θ_3 as the design progresses. In this case, the design begins with a wash-out design and rapidly progresses to a wash-in design. After eight design cycles, the laminate-ply orientations change little during the ensuing design process.

Figure 12 shows the progress of both hinge-moment reduction and augmented-performance index reduction with each automated design cycle. The sharp reductions in the performance index (visible, for instance, between cycle numbers 10 and 11) are due to reductions in the value of the user-chosen constant r_p in Eq. (21). Note also that these results were obtained from a mostly automated procedure. An interactive, human/machine approach would substantially reduce the number of cycles necessary to achieve the same results.

Because the initial results obtained when the aileron flap-to-chord ratio and spanwise location were design parameters show the presence of two local minima, it is not clear that this local minimum located by the optimization driver is a global minimum. Because of this, several other sets of initial conditions were tried. However, the final results obtained were very similar and insensitive to initial conditions.

Conclusions

The simultaneous optimization of structural stiffness (through laminate orientation), aileron size, and aileron spanwise location to obtain hinge-moment reduction has been demonstrated and discussed. The configuration to which the procedure was applied, although unsophisticated, still displays essential aeroelastic features of a real-world configuration. When the aileron chord and spanwise location are treated as fixed design parameters, as opposed to design variables, the minimum hinge moment required to achieve a specified roll effectiveness has two local minima, one of which is a global minimum. Structural optimization of the configuration with a fixed control-surface geometry and position requires a trade-off between aileron rolling power and damping-in-roll of the wing planform itself.

When aileron spanwise location and flap-to-chord ratio are included as design variables, further design-sensitivity information must be available. This sensitivity information involves differentiation to compute the changes in aileron hinge moment (including aeroelastic effects) with respect to flap-to-chord ratio and aileron spanwise position. Once this is done, optimization is straightforward.

There are any number of configurations to which this methodology may be applied. For each configuration, the topographical characteristics of the design space will be quantitatively different than those shown in this study. However, it is likely that the essential aeroelastic features of the present configuration will carry over to realistic designs. Given the intricacy of the complex process that occurs during the design of a realistic, effective control surface, the mathematical effort demonstrated here may not be inexpensive. However, the present results indicate that a combined synergistic effort can produce a more effective design than that produced by solitary processes. Furthermore, such a combined effort recognizes the aeroelastic features of the problem that tightly bind the two disciplines of structural design and control design.

Acknowledgments

The authors gratefully acknowledge the support of this research effort by NASA/Langley Research Center under Grant NSG-1-157, with Boyd Perry III as technical monitor.

References

[1]Cubick, F. E. C., and Jex, H. R., "Aerodynamics, Stability and Control of the 1903 Wright Flyer," National Air and Space Museum, Washington, DC, 1987, pp. 19–43.

[2]Cox, H. R., and Pugsley, A. G., "The Aileron Power of the Monoplane," Aeronautical Res. Council, R. & M. 1640, April 1934.

[3]Ogawa, T., "A Design Formula for Ailerons," Aeronautical Res. Institute, Rept. 88, Tokyo Imperial Univ., Tokyo.

[4]Irving, H. B., Ower, E., and Hankins, G. A., "An Investigation of the Aerodynamic Properties of Wing Ailerons, Part I," Aeronautical Res. Council, R. & M. 550, 1918.

[5]Glauert, H., "The Effect of Aspect Ratio and Shape of Wing Tip on Aerofoil Characteristics," Aeronautical Res. Council, R. & M. 575, 1919.

[6]Harmon, S. M., "Determination of the Effect of Wing Flexibility on Lateral Maneuverability and a Comparison of Calculated Rolling Effectiveness with Flight Results," NACA (Advanced Restricted Rept.) ARR 4A28, L-525 Jan. 1944.

[7]Bisplinghoff, R. L., Ashley, H., and Halfman, R. L., *Aeroelasticity*, Addison-Wesley, Reading, MA, 1955.

[8]Shirk, M. H., Hertz, T. J., and Weisshaar, T. A., "Aeroelastic Tailoring – Theory, Practice, Promise," *Journal of Aircraft*, Vol. 23, No. 1, 1986, pp. 6–18.

[9]Weisshaar, T. A., "Aeroelastic Tailoring – Creative Uses of Unusual Materials," AIAA Paper 87-117, Monterey, CA, April 1987.

[10]Love, M. H., Milburn, R. T., and Rogers, W. A., "Some Considerations for Integrating Aeroelasticity into CAE," ASME Winter Annual Meeting, Boston, MA, Dec. 1987.

[11]Sensburg, O., and Schmidinger, G., "Integrated Design of Structures," Flight Mechanics Symp., Improvement of Combat Performance for Existing and Future Aircraft, Treviso, Italy, April 1986.

[12]Gray, W. L., and Schenk, K. L., "A Method for Calculating the Subsonic Steady-State Loading on an Airplane with a Wing of Arbitrary Plan Form and Stiffness," NACA TN 3030, 1953.

[13]Weisshaar, T. A., "Forward Swept Wing Static Aeroelasticity," Air Force Flight Dynamics Lab., Wright-Patterson AFB, OH, AFFDL-TR-79-3087, June 1979.

[14]Etkin, B. E., *Dynamics of Atmospheric Flight,* Wiley, New York, 1972, pp. 310, 311.

[15]*USAF Stability and Control Datcom,* Flight Control Div., Flight Dynamics Lab., Wright-Patterson AFB, OH, Oct. 1960 (revised Jan. 1974), Chap. 6.

[16]Theodorsen, T., and Garrick, I. E., "Nonstationary Flow About a Wing-Aileron-Tab Combination, Including Aerodynamic Balance," NACA TR 736, 1942.

[17]Rao, S. S., *Optimization-Theory and Applications,* Wiley Eastern Ltd., New Delhi, 1985, pp. 310–318, 392-405.

[18]Niblett, L. T., "Aileron Reversal of Swept Wings with Crossflexibilities," T. R. 83023, Royal Aircraft Establishment, Feb. 1983.

Recommended Reading from the AIAA Progress in Astronautics and Aeronautics Series . . . AIAA

Thermophysical Aspects of Re-Entry Flows

Carl D. Scott and James N. Moss, editors

Covers recent progress in the following areas of re-entry research: low-density phenomena at hypersonic flow conditions, high-temperature kinetics and transport properties, aerothermal ground simulation and measurements, and numerical simulations of hypersonic flows. Experimental work is reviewed and computational results of investigations are discussed. The book presents the beginnings of a concerted effort to provide a new, reliable, and comprehensive database for chemical and physical properties of high-temperature, nonequilibrium air. Qualitative and selected quantitative results are presented for flow configurations. A major contribution is the demonstration that upwind differencing methods can accurately predict heat transfer.

TO ORDER: **Write, Phone, or FAX:** AIAA c/o TASCO, 9 Jay Gould Ct., P.O. Box 753, Waldorf, MD 20604 Phone (301) 645-5643, Dept. 415 ■ FAX (301) 843-0159

Sales Tax: CA residents, 7%; DC, 6%. For shipping and handling add $4.75 for 1–4 books (call for rates for higher quanties). Orders under $50.00 must be prepaid. Foreign orders must be prepaid. Please allow 4 weeks for delivery. Prices are subject to change without notice. Returns will be accepted within 15 days.

1986 626 pp., illus. Hardback
ISBN 0-930403-10-X
AIAA Members $59.95
Nonmembers $84.95
Order Number V-103